RSC Advances

PAPER

View Article Online
View Journal | View Issue

Cite this: *RSC Adv.*, 2014, **4**, 41572

Multifunctional iron oxide/silk-fibroin (Fe_3O_4–SF) composite microspheres for the delivery of cancer therapeutics†

Haiyun Zhang, Xilan Ma,* Chuanbao Cao,* Meina Wang and Youqi Zhu

Received 18th June 2014
Accepted 11th August 2014

DOI: 10.1039/c4ra05919k

www.rsc.org/advances

In this article, we report novel multifunctional iron oxide/silk-fibroin (Fe_3O_4–SF) microspheres synthesized by simple salting out process. These microspheres are used as the carriers of doxorubicin hydrochloride (a traditional anti-cancer drug), denoted as DOX–Fe_3O_4–SF. The results show that the drug loading capacity (LC) is 3.3% and the drug encapsulation efficiency (EE) could reach up to 76%. The DOX-loaded microspheres exhibit sustained and pH-sensitive release patterns. The total DOX release is measured to be about 60% at pH 5.5. More interestingly, RhB-labelled Fe_3O_4–SF microspheres exhibit a striking endocytosis, selectively accumulating in the cytoplasm compared to the free RhB. The endocytosis of DOX–Fe_3O_4–SF microspheres results in only ~10% survival ratio of HeLa cells after 48 h. Furthermore, because of the remarkable biocompatibility of SF, Fe_3O_4–SF microspheres show no cytotoxicity toward HeLa cells compared to DOX–Fe_3O_4–SF. The results clearly indicate that Fe_3O_4–SF microspheres hold significant potential for drug loading and delivery into cancer cells to induce cell death.

1 Introduction

Since last few centuries, cancer remains a major health problem worldwide. Statistical results have confirmed that ~25% of mortality rate[1] is due to cancer in United States. Outside this awful truth, fortunately, cancer-therapy drugs have been proposed to be efficient treatment strategy in a controllable release manner.[2–4] However, cancer-therapy drugs are often accompanied with toxic side effects and suffer from a low targeted drug delivery efficiency. It is still a significant challenge to transport anti-cancer drugs accurately to the targeted area for avoiding the damage of healthy tissues.[5–7] This issue has attracted considerable interest in the synthesis of appropriate drug delivery system with high tumour targeting efficiency.

Nanostructured magnetic Fe_3O_4 (Fe_3O_4 NPs), widely used in various biomedical fields due to biocompatibility, can provide potential platform for targeted drug delivery. Forced by external (or internally implanted) magnetic fields, magnetic nanoparticles can be manipulated to selectively target the affected organs or tissues.[8–14] However, despite these advantages, it is important to understand the toxicity of Fe_3O_4 NPs. Some reports have found that excess accumulation of iron ions would cause neuronal damage in the brain or could affect protein synthesis in neural cells.[15–17] For improving the cytocompatibility of Fe_3O_4 NPs, combining with carriers to form multifunctional composites is required. Multifunctional composites are potential platforms for many applications such as cancer therapy. Moreover, such a magnetic composite could be used for bioimaging purposes in the treatment of hyperthermia.[18] Several ligands have been developed to improve multifunctional drug delivery, for example, silica and organic polymers.[19,20] Yanna Cui *et al.* have demonstrated that the magnetic PLGA NPs loaded with DOX are effective for brain glioma treatment. Jinjin Shi *et al.* reported PEGylated fullerene multi-functional magnetic nanocomposites to be a possible cure for cancer theranostic.[21,22] These results indicate that this kind of multifunctional composites is very promising for targeted drug delivery. However, most targeting ligands are synthetic polymers and are difficult to modify. On the other hand, natural polymers have attracted attention primarily because they are similar to biological macromolecules, are often biocompatible or even biodegradable, and relatively inexpensive, which allows the potential for chemical or physical modification.[23,24]

As a natural, fibrous protein produced by a variety of insects and spiders, silk fibroin is used for drug delivery with sustainable release properties. In particular, silk fibroin's superior biocompatibility compared to synthetic macromolecules and its controllable degradability, make it a preferred biomedical material.[25,26] Above all, silk has a negative charge because it comprises 39% glycine and 34% alanine[27] in solution with a pH of >4. In addition, the cytocompatibility of Fe_3O_4 NPs increases because the surface charge of magnetic NPs decreases by combination with SF.[28] Thus, it is of great significance to prepare multifunctional iron oxide/silk-fibroin composites for

Research Centre of Materials Science, School of Materials Science and Engineering, Beijing Institute of Technology, Beijing 100081, P. R. China. E-mail: maxilan@bit.edu.cn; cbcao@bit.edu.cn; Fax: +86 10 68912001; Tel: +86 10 68913792

† Electronic supplementary information (ESI) available. See DOI: 10.1039/c4ra05919k

drug delivery. In fact, the preparation of magnetic silk composites was reported in 1998 (ref. 29) and it is significant in scientific research. However, their main focus was on the modification of spider silk fibers. Recently, Fe_3O_4 NPs coated with SF have been reported but the report mostly focused on the modification of Fe_3O_4 NPs by SF solution. There are a limited number of reports on exploring the conjugation of SF and Fe_3O_4 NPs to obtain multifunctional composites for potential targeted drug delivery. On the other hand, designing a composite with selectivity to cells, although challenging, is of considerable importance for research and therapy of several serious diseases.[30,31] Fe_3O_4–PEG–FITC–CNT composites have been reported to be located at the perinuclear region of MCF7 cells[18,32] but the synthetic methods of the composites are complex. Efforts have been made to investigate the endocytosis of silk composites but there are few reports on multifunctional iron oxide/silk-fibroin composites. For example, Shuying Yu[33] *et al.* prepared FUDR-loaded SF nanospheres but endocytosis experiment showed the nanocarriers only adhere onto the HeLa cells. Joydip Kundu[34] *et al.* reported silk nanoparticles prepared by desolvation could be endocytosed by cells. However, targeted agents (such as Fe_3O_4 NPs) were not found in silk nanoparticles and they might not actively target cancerous cells. Therefore, simple synthesis of multifunctional iron oxide/silk-fibroin composites and the composites could be endocytosed by HeLa cells are required for the potential of targeted drug delivery.

Herein, novel multifunctional iron oxide/silk-fibroin composites are fabricated *via* a simple salting out process. Doxorubicin hydrochloride (DOX) is loaded onto the Fe_3O_4–SF microspheres and the drug release properties are examined. More importantly, we were surprised to find that the multifunctional iron oxide/silk-fibroin composites exhibited a excellent endocytosis and could selectively accumulate in the cytoplasm of HeLa cells. The effects of these composite microspheres on cell cytotoxicity were also evaluated by HeLa cells.

2 Experimental

2.1 Silk fibroin solutions

Bombyx mori fibroin solution was prepared according to previously published procedures.[35–38] Silk was boiled for 30 minutes in 0.02 M Na_2CO_3 solution and the same procedure was repeated twice to degum the glue-like sericin coating. The extracted silks fibroin was dissolved in $CaCl_2/H_2O/CH_3CH_2OH$ solution (mole ratio, 1 : 8 : 2) at 80 °C. Then, the fibroin solution was dialyzed with dialysis cassettes (molecular weight cut-off, 14 000) against distilled water for 3 days to yield fibroin aqueous solution.

2.2 Synthesis of Fe_3O_4 nanoparticles

In the experiment, $Fe_2(SO_4)_3$ (17.5 ml, 0.25 mol l^{-1}) and $FeSO_4$ (10 ml, 0.5 mol l^{-1}) were mixed in a single-neck flask. $NH_3 \cdot H_2O$ was added to the solution and the pH of the solution was adjusted to ~10.[39] The mixture was magnetically stirred for 30 minutes and kept at room temperature for a week. Then, the resultant black solution was matured for 30 minutes at 80 °C. The precipitate was washed thoroughly with distilled water and ethanol. Nanoparticles were obtained after drying at 60 °C in vacuum oven.

2.3 Synthesis of Fe_3O_4–SF, DOX–Fe_3O_4–SF and RhB-labelled Fe_3O_4–SF microspheres

Fe_3O_4–SF microspheres were prepared by mixed solution salting out from potassium phosphate (pH = 9).[40] 0.5 wt% SF solution and 0.5 wt% Fe_3O_4 solution were mixed in a volume ratio of 40 : 1. Then, the mixed solution was added to 1.25 M potassium phosphate solution in a volume ratio of 1 : 5. The mixture was incubated at 4 °C for 2 h and kept at room temperature for 12 h. The precipitate was collected and washed thoroughly with distilled water. Fe_3O_4–SF microspheres were obtained by freeze-drying.

Preparation process of DOX–Fe_3O_4–SF microspheres was simple. Fe_3O_4–SF microspheres (80 mg per 10 ml) dispersed into PBS were mixed with different concentrations of DOX solution (0.15, 0.25, 0.35 and 0.5 mg ml^{-1}). The mixed system was stirred at room temperature for 12 h, and then the precipitate was collected and washed thoroughly with PBS to remove residual DOX. Composites were obtained by freeze-drying. The collected supernatant was analyzed by UV-vis spectrometry to calculate drug loading capacity (LC) and drug encapsulation efficiency (EE). LC and EE was calculated as follows:

$$\mathrm{LC}(\%) = \frac{\text{The amount of drugs by adsorption}}{\text{The amount of carriers}} \times 100$$

$$\mathrm{EE}(\%) = \frac{\text{initial amount of drugs} - \text{drugs in supernatant}}{\text{initial amount of drugs}} \times 100$$

RhB-labelled composite microspheres were prepared by adsorption. Fe_3O_4–SF microspheres (80 mg per 10 ml) dispersed into PBS were mixed with RhB solution (0.15 mg ml^{-1}). The mixed system was stirred at room temperature for 12 h, the precipitate was collected and washed thoroughly with PBS to remove residual RhB. Composites were obtained by freeze-drying.

2.4 Characterization

The shapes and crystalline structures of Fe_3O_4 NPs were characterized by transmission electron microscopy (TEM) and high resolution transmission electron microscopy (HRTEM). The magnetic property of the samples was investigated by vibrating sample magnetometer (VSM). The morphology of the composite microspheres was analyzed by scanning electron microscopy (SEM). X-ray diffraction (XRD) curves were recorded to analyze the crystalline structure of samples.

2.5 *In vitro* drug release

DOX–Fe_3O_4–SF microspheres (50 mg) and PBS (10 ml, pH = 5.5, 7.4) were added to the dialysis cassettes. Dialysis cassettes were sealed at both the ends and immersed into 90 ml PBS (pH = 5.5, 7.4, 37 °C). At set time increments, 10 ml of the supernatant was

collected and replaced with an equal volume of fresh PBS solution. The collected supernatant was analyzed by UV-vis spectrometry.

2.6 Cellular uptake investigation

Laser confocal investigation was applied to examine the localization of composite microspheres into cells. The free RhB and RhB-labelled Fe_3O_4–SF microspheres were added to HeLa cells and were co-cultured for 4 h. Then, the cells were washed three times with PBS to eliminate residues. The cells were then fixed with 4% paraformaldehyde for 15 minutes. Finally, the cells were analyzed for red fluorescence by a confocal microscope.

2.7 MTS assay

The cell metabolic activity was measured by MTS. HeLa cells were maintained in DMEM medium supplemented with 10% fetal bovine serum. The cells were cultured at 37 °C in a humidified atmosphere with 5% CO_2. HeLa cells in accordance with the density of 5000 cells per well were seeded in 96-well plates. Medium (100 μl) prepared with different concentrations of the sample solution (200, 100, 50, 25, 12.5, 6.25 and 3.125 μg ml^{-1}) was added to each well. The cells with medium were cultured for 24 h and 48 h at 37 °C. 20 μl MTS was added to each well and the system was maintained for 4 h, then the absorbance of each well was determined at 490 nm.

3 Results and discussion

3.1 Fe_3O_4 NPs structural analysis

Fig. 1a shows the TEM image of the as-prepared Fe_3O_4 NPs. The size distribution of Fe_3O_4 NPs is uniform and the mean diameter size is 15 ± 2 nm (Fig. 1a). To test the crystalline properties of magnetic nanoparticles, high resolution transmission electron microscopy (HRTEM) analysis was performed. In HRTEM images of Fig. 1b, the lattice fringes were clearly observed and the result showed Fe_3O_4 NPs hold good crystalline properties. The phase identification of Fe_3O_4 NPs was characterized by XRD. Strong diffraction peaks were observed corresponding to the crystal planes of (220), (311), (400), (422), (511) and (440) of crystalline Fe_3O_4 NPs (Fig. 1c). The results showed that Fe_3O_4 NPs held the *trans*-spinel phase structure. Magnetization measurements recorded with VSM were performed to examine the magnetic behavior of Fe_3O_4 NPs. In Fig. 1d, the specific saturation magnetization value of Fe_3O_4 NPs was measured to be 70.15 emu g^{-1}, and no magnetic hysteresis was observed. These results demonstrate that Fe_3O_4 NPs are superparamagnetic as previously reported.[41,42]

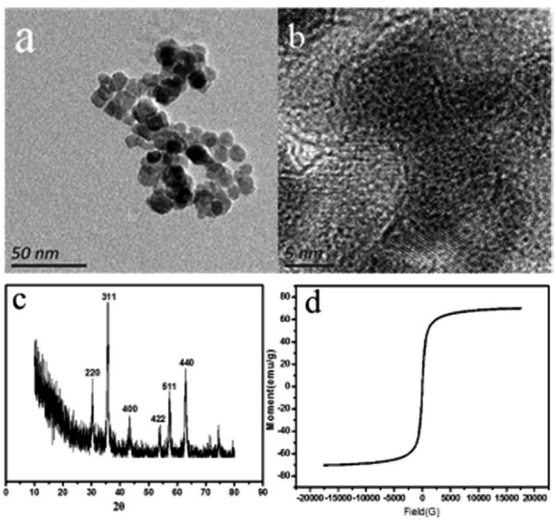

Fig. 1 TEM images of the as-prepared Fe_3O_4 NPs (a), HRTEM images (b), XRD of the as-prepared Fe_3O_4 NPs (c) and hysteresis loops of the as-prepared Fe_3O_4 NPs (d).

3.2 Morphology and properties of Fe_3O_4–SF microspheres

Fig. 2a depicts the SEM image of the composite microspheres. The aqueous-derived microspheres showed a relatively rough surface with size ranging from 500 ± 50 to 3000 ± 200 nm. Some small bumps were found on the surface, which might be caused by iron oxide aggregation. To verify this hypothesis, the composites were measured by TEM and HRTEM. From Fig. 2c, inhomogeneous distribution of Fe_3O_4 NPs in composites could be clearly found. This phenomenon result from the magnetic attraction force of Fe_3O_4 NPs. However, clear lattice fringes and uniform size distribution of Fe_3O_4 NPs demonstrated that magnetic nanoparticles were not affected by silk (Fig. 2d). Fig. 2b showed the surface of composites had no obvious change after loading DOX. This might be because a small amount of DOX was absorbed into microspheres. To investigate changes in structure of silk, XRD analysis was employed. In

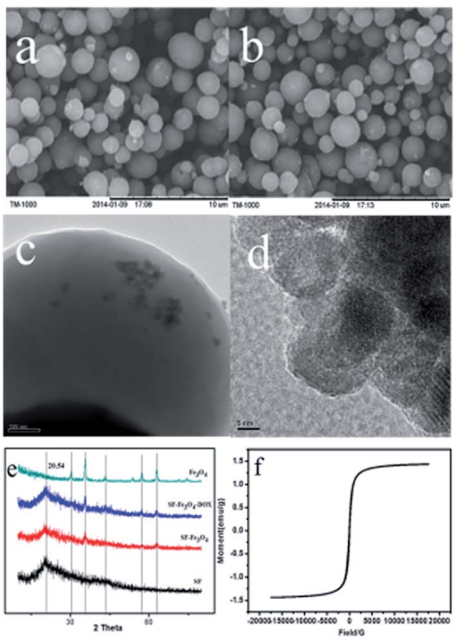

Fig. 2 Morphology of Fe_3O_4–SF (a) and after loading DOX (b), TEM images (c) and HRTEM images (d) of the as-prepared Fe_3O_4–SF, XRD of as-prepared composite microspheres (e) and hysteresis loops of DOX–Fe_3O_4–SF composite microspheres (f).

Fig. 2e, all the microspheres exhibited a mostly β-sheet structure ($2\theta = 20.5°$) and a similar crystalline properties. The results indicated that silk II crystalline structure existed in the composites and Fe_3O_4 NPs had no effect on silk structure. Magnetic behavior of the composites was examined by VSM. The saturated magnetization was about 1.5 emu g^{-1}, and no magnetic hysteresis was observed in Fig. 2f. The saturated magnetization of composites was smaller than pure Fe_3O_4 NPs because a small amount of magnetic nanoparticles was added to the silk solution. The quality percentage of Fe_3O_4 NPs was analyzed by TGA (Fig. S1†). Therefore, we have successfully synthesized magnetic iron oxide/silk-fibroin composite microspheres and the composites provide possibility for targeted drug delivery.

3.3 Loading efficiency

The drug loading capacity (LC) and drug encapsulation efficiency (EE) are important to evaluate the availability of the carriers. As shown in Fig. 3, different concentrations of DOX solution were used to obtain the appropriate LC and EE. LC increased with increasing DOX concentration but the EE decreased under the same conditions. According to the trends of curves, LC could reach to the biggest point under one DOX concentration. Whereas the EE changed smaller than the former and could not conform to the requirements of the cost. Therefore, the suitable DOX concentration was 0.35 mg ml^{-1}, and the LC and EE were 3.3%, 76%, respectively.

3.4 *In vitro* drug release

pH is an important factor[43] because it exists naturally in the cells of pathological change, as well as cancer cells. Therefore, DOX release at different pH was investigated. As shown in Fig. 4, DOX–Fe_3O_4–SF microspheres exhibited a sensitive response to pH. The *in vitro* release showed that about 60% of DOX was released at pH 5.5, whereas DOX release was less than 20% at pH 7.4 under the same conditions. This might result from the presence of strong hydrogen bonding force interactions between the composites and DOX at pH 7.4. Under acidic conditions,[44] H^+ in solution could compete with the hydrogen bond forming group and weaken hydrogen bond interactions. Furthermore, both DOX and silk carry positive charge in H^+ solution, which provides the necessary repulsion between them. Thus, DOX release was greater at pH 5.5 than 7.4. Otherwise, DOX released from the composites was sustained for a long time. These results demonstrate the Fe_3O_4–SF composite microspheres could be used for drug delivery.

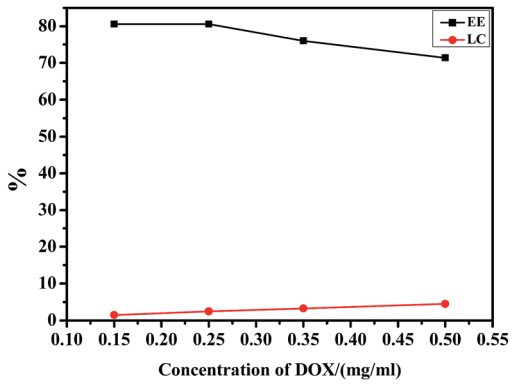

Fig. 3 Drug loading capacity (LC) and drug encapsulation efficiency (EE) under different DOX concentrations.

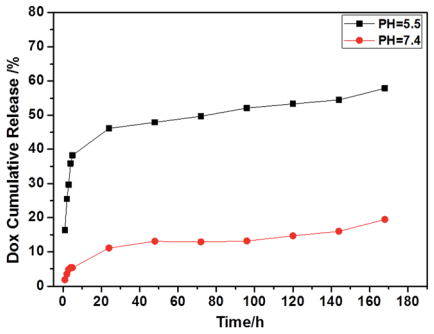

Fig. 4 DOX released from DOX–Fe_3O_4–SF composite microspheres under different pH conditions.

3.5 Confocal assay

The uptake of the RhB-labelled composite microspheres by HeLa cells was observed using fluorescence and confocal microscopy. Fig. 5(c) and (d) showed that the cellular cytoplasm was stained with red fluorescence soon after 4 h of incubation, revealing cellular internalization of the RhB-labelled composite microspheres. It was clearly visible that the red fluorescence in cellular cytoplasm was focused on together, which result from

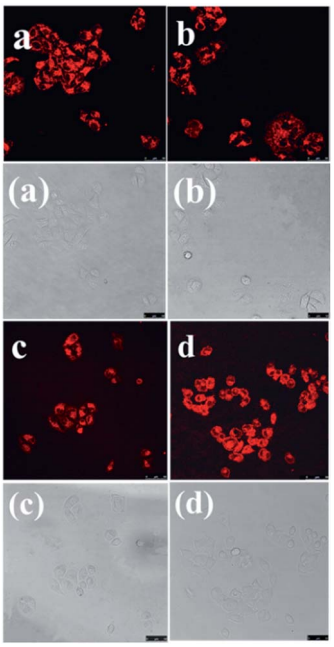

Fig. 5 Confocal microscopic images of HeLa cells with free RhB (a and b) and RhB-labelled composite microspheres (c and d) (12.5 μg ml^{-1}) in different regions.

the magnetic attraction of Fe_3O_4–SF composites. In contrast, cells treated with free RhB showed discursive red fluorescence internalized in the cellular cytomembrane and cytoplasm. These results indicated that the RhB-labelled composite microspheres could be uptaken by HeLa cells. Interestingly, the cells remained viable after incubation with for 4 h. The results verify that composite microspheres have no cytotoxicity effect on HeLa cells. Compared with previous studies, we have successfully synthesized multifunctional iron oxide/silk-fibroin composites and the composites could be uptaken by HeLa cells, which provides potential for the targeted drug delivery.

3.6 MTS assay

To verify whether the released DOX was pharmacologically active, the cytotoxic effect of the DOX–Fe_3O_4–SF composite microspheres on HeLa cells was investigated. Fig. 6 showed the viability of HeLa cells incubated with Fe_3O_4–SF and DOX–Fe_3O_4–SF composite microspheres for 24 h and 48 h. The results showed that the cytotoxicity of DOX–Fe_3O_4–SF increased with the increase in concentrations and DOX–Fe_3O_4–SF held greater cytotoxicity than Fe_3O_4–SF. On the other hand, only ~10% HeLa cells survived after co-culture with DOX–Fe_3O_4–SF for 48 h. This might be attributed to the release of DOX inside cells. Otherwise, the cytotoxicity of DOX–Fe_3O_4–SF increased with the increase of exposure on cells. This might be because more DOX was released inside the cells with increasing time. Interestingly, Fe_3O_4–SF exhibited no indication of cytotoxicity on HeLa cells due to the remarkable biocompatibility of silk fibroin. The results showed multifunctional Fe_3O_4–SF composite microspheres hold significant potential for targeted drug delivery.

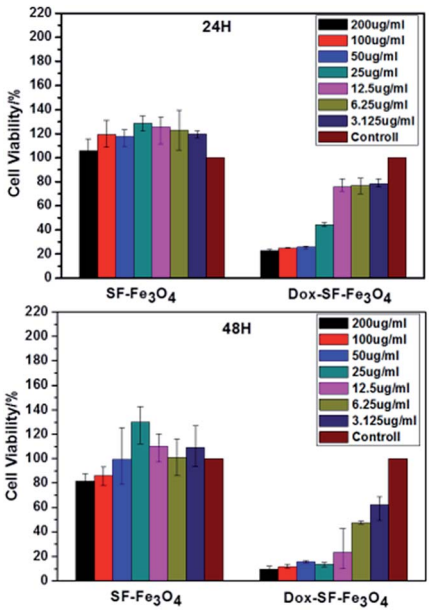

Fig. 6 Effect of composite microspheres on the viability of HeLa cells, as measured by MTS.

4 Conclusions

In summary, we suggest novel multifunctional iron oxide/silk-fibroin composite microspheres prepared *via* a simple salting out process. DOX was successfully loaded into Fe_3O_4–SF composite microspheres, which presented sustained and pH-sensitive release patterns. The total DOX release is measured to be about 60% at pH = 5.5. More interestingly, the multifunctional iron oxide/silk-fibroin composites exhibited a striking endocytosis and could selectively accumulate in the cytoplasm of HeLa cells, which provided the possibility for research and therapy of several serious diseases. MTS results reveal that Fe_3O_4–SF microspheres with different concentrations had no cytotoxicity due to the remarkable biocompatibility of silk fibroin. However, DOX–Fe_3O_4–SF microspheres exhibit greater cytotoxicity toward HeLa cells and only ~10% HeLa cells survived after 48 h incubation due to the release of DOX inside cells. The results clearly indicate that the Fe_3O_4–SF microspheres hold significant potential in the application of targeted drug delivery.

References

1 R. Siegel, D. Naishadham and A. Jemal, *Ca-Cancer J. Clin.*, 2013, **63**, 11.
2 Y. Chen, H. R. Chen, S. J. Zhang, F. Chen, L. X. Zhang, J. M. Zhang, M. Zhu, H. X. Wu, L. M. Guo, J. W. Feng and J. L. Shi, *Adv. Funct. Mater.*, 2011, **21**, 270.
3 L. E. Vlerken and M. M. Amiji, *Expert Opin. Drug Delivery*, 2006, **3**, 205.
4 P. Huang, Z. M. Li, J. Lin, D. P. Yang, G. Gao, C. Xu, L. Bao, C. L. Zhang, K. Wang, H. Song, H. Y. Hu and D. X. Cui, *Biomaterials*, 2011, **32**, 3447.
5 L. L. Li, Y. Q. Guan, H. Y. Liu, N. J. Hao, T. L. Liu, X. W. Meng, C. H. Fu, Y. Z. Li, Q. L. Qu, Y. G. Zhang, S. Y. Ji, L. Chen, D. Chen and F. Q. Tang, *ACS nano*, 2011, **5**, 7462.
6 B. Subia, S. Chandra, S. Talukdar and S. C. Kundu, *Integr. Biol.*, 2014, **6**, 203.
7 S. D. Steichen, M. C. Moore and N. A. Peppas, *Eur. J. Pharm. Sci.*, 2013, **48**, 416.
8 F. Danhier, O. Feron and V. Préat, *J. Controlled Release*, 2010, **148**, 135.
9 T. Lammers, W. E. Kiessling and G. Storm, *Mol. Pharmacol.*, 2010, **7**, 1899.
10 C. H. Wang, S. T. Kang and C. K. Yeh, *Biomaterials*, 2013, **34**, 1852.
11 L. P. Mazor, G. R. Dakwar, M. Popov, S. Kolusheva, A. Shames, C. Linder, S. Greenberg, E. Heldman, D. Stepensky and R. Jelinek, *Int. J. Pharm.*, 2013, **450**, 241.
12 J. M. Hu, Y. F. Qian, X. F. Wang, T. Liu and S. Y. Liu, *Langmuir*, 2012, **28**, 2073.
13 K. J. Thompson, S. Shoham and J. R. Connor, *Brain Res. Bull.*, 2011, **55**, 155.
14 J. D. Blackwell, V. I. Shubayev, R. R. Fiñones and S. G. Jin, *Biomaterials*, 2007, **28**, 2572.
15 K. J. Thompson, S. Shoham and J. R. Connor, *Brain Res. Bull.*, 2001, **55**, 155.

16 L. Zecca, M. B. H. Youdim, P. Riederer, J. R. Connor and R. R. Crichton, *Nat. Rev. Neurosci.*, 2004, **5**, 863.
17 T. R. I. I. Pisanic, J. D. Blackwell, V. I. Shubayev, R. R. Finones and S. Jin, *Biomaterials*, 2007, **28**, 2572.
18 J. J. Khandare, A. J. Badhwar, S. D. Satavalekar, S. G. Bhansali, N. D. Aher, F. Kharas and S. S. Banerjee, *Nanoscale*, 2012, **4**, 837.
19 J. Lu, M. Liong, Jeffrey I. Zink and F. Tamanoi, *Small*, 2007, **3**, 1341.
20 H. Freichels, F. Danhier, V. Préat, P. Lecomte and C. Jérôme, *Int. J. Artif. Organs*, 2011, **34**, 152.
21 J. J. Shi, X. Y. Yu, L. Wang, Y. Liu, J. Gao, J. Zhang, R. Ma, R. Y. Liu and Z. Z. Zhang, *Biomaterials*, 2013, **34**, 9666.
22 N. Schleich, P. Sibret, P. Danhier, B. Ucakar, S. Laurent, R. N. Muller, C. Jérôme, B. Gallez, V. Préat and F. Danhier, *Int. J. Pharm.*, 2013, **447**, 94.
23 P. B. Malafaya, G. A. Silva, R. L. Reis, P. B. Malafaya, G. A. Silva and R. L. Reis, *Adv. Drug Delivery Rev.*, 2007, **59**, 207.
24 J. A. Kluge, O. Rabotyagova, G. G. Leisk and D. L. Kaplan, *Trends Biotechnol.*, 2008, **26**, 244.
25 C. Veparia and D. L. Kaplan, *Prog. Polym. Sci.*, 2007, **32**, 991.
26 Q. Lv, C. B. Cao, Y. Zhang, X. L. Ma and H. S. Zhu, *J. Mater. Sci.: Mater. Med.*, 2004, **15**, 1193.
27 G. X. Zhang and C. Li, *Acta Sericol. Sin.*, 2009, **35**, 99.
28 D. H. Yan, G. F. Yin, Z. B. Huang, M. Yang, X. M. Liao, Y. Q. Kang, Y. D. Yao, B. Q. Hao and D. Han, *J. Phys. Chem. B*, 2009, **113**, 6047.
29 E. L. Mayes, F. Vollrath and S. Mann, *Adv. Mater.*, 1998, **10**, 801.
30 B. Kang, M. A. Mackey and M. A. El-Sayed, *J. Am. Chem. Soc.*, 2010, **132**, 1517.
31 L. Rajendran, H. J. Knolker and K. Simons, *Nat. Rev. Drug Discovery*, 2010, **9**, 29.
32 D. Depan and R. D. K. Misra, *Nanoscale*, 2012, **4**, 6325.
33 S. Y. Yu, W. H. Yang, S. Chen, M. J. Chen, Y. Z. Liu, Z. Z. Shao and X. Chen, *RSC Adv.*, 2014, **4**, 18171.
34 J. Kundu, Y. Il Chung, Y. H. Kim, G. Tae and S. C. Kundu, *Int. J. Pharm.*, 2010, **388**, 242.
35 J. Zhou, C. B. Cao and X. L. Ma, *Int. J. Biol. Macromol.*, 2009, **45**, 504.
36 X. H. Zhang, C. B. Cao, X. L. Ma and Y. N. Li, *J. Mater. Sci.: Mater. Med.*, 2012, **23**, 315.
37 Q. Lu, S. J. Zhang, K. Hua, Q. L. Feng, C. B. Cao and F. Z. Cui, *Biomaterials*, 2007, **28**, 2306.
38 J. Zhou, C. B. Cao, X. L. Ma and J. Lin, *Int. J. Biol. Macromol.*, 2010, **47**, 514.
39 S. Laurent, D. Forge, M. Port, A. Roch, C. Robic, L. V. Elst and R. N. Muller, *Chem. Rev.*, 2008, **108**, 2064.
40 A. S. Lammel, X. Hu, S. H. Park, D. L. Kaplan and T. R. Scheibel, *Biomaterials*, 2010, **31**, 4583.
41 M. V. Kovalenko, M. I. Bodnarchuk, R. T. Lechner, G. Hesser, F. Schäffler and W. Heiss, *J. Am. Chem. Soc.*, 2007, **129**, 6352.
42 F. X. Redl, C. T. Black, G. C. Papaefthymiou, R. L. Sandstrom, M. Yin, H. Zeng, C. B. Murray and S. P. O'Brien, *J. Am. Chem. Soc.*, 2004, **126**, 14583.
43 R. Cheng, F. H. Meng, C. Deng, H. A. Klok and Z. Y. Zhong, *Biomaterials*, 2013, **34**, 3647.
44 B. Subia, S. Chandra, S. Talukdar and S. C. Kundu, *Integr. Biol.*, 2014, **6**, 203.